Modeling the sound generated by underwater bubbles.

Suhas Jain Suresh: AA201A Project Report

June 8, 2018

Abstract

Sounds generated by underwater bubbles is an important phenomenon and has been studied for over many decades. The aim of this project is to systematically derive the reduced-order models used to study sounds generated by underwater bubbles. Procedure to synthesize the sound using these models will be described.

1 Introduction

Sound generated by underwater bubbles has wide range of passive and active acoustic sensing applications and has been an active research area for almost a century starting with the monumental contributions by Rayleigh (1917), Minnaert (1933), Strasberg (1953). While most of the previous studies were theoretical and experimental (Leighton 2012), a successful computational approach (a direct computation of sound) hasn't been performed yet for other than a single or at-most multiple bubbles of simple configurations due to its inherent cost and accuracy requirements. An alternative approach is to model the sound generated by bubbles with incompressibility approximations and using reduced-order models for bubble vibration behavior (such as a spring-mass-damper system). This approach eliminates the acoustic CFL constraints of the compressible solution techniques and makes it cost effective and computationally feasible. These techniques have also recently sought attention in the graphics community (Langlois et al. 2016).

2 Spring-mass-damper system

A bubble in a liquid when excited by an external force (a pressure impulse) oscillates. This oscillation has many modes, out of which the zeroth-order mode (also called as a breathing mode) is the predominant one (see, Section 3) where the bubble pulsates with its volume oscillating about its mean in an approximately simple harmonic motion. Hence a simple spring-mass-damper analogy can be brought in to study this mechanism with spring being the gas inside the bubble, mass being the inertia due to the gas and surrounding liquid and damping due to viscous effects, thermal conduction and the radiation of sound itself.

2.1 Frames of reference

The equation of motion of a bubble in this reduced-order model of spring-mass-damper system can be expressed in four different frames of reference. If the bubble is excited by a force F or an equivalent pressure P, then the response of the bubble can be expressed in terms of the radius of the bubble as a function of time $R(t) = R_0 - R_\epsilon e^{i\omega_o t}$ or as an equivalent spherical volume $V(t) = V_0 - V_\epsilon e^{i\omega_o t}$, where R_0 and V_0 are the equivalent radius and volumes, R_ϵ and V_ϵ are the amplitude of radius and volume change, negative sign implies that the radius and volume reduces with the increase in pressure or force. Then the four frames of reference can be written as

1. *radius-pressure* frame
$$m_{rp}R''_\epsilon + b_{rp}R'_\epsilon + k_{rp}R_\epsilon = Pe^{i\omega t} \tag{1}$$
2. *volume-pressure* frame
$$m_{vp}V''_\epsilon + b_{vp}V'_\epsilon + k_{vp}V_\epsilon = Pe^{i\omega t} \tag{2}$$
3. *radius-force* frame
$$m_{rf}R''_\epsilon + b_{rf}R'_\epsilon + k_{rf}R_\epsilon = Fe^{i\omega t} \tag{3}$$

4. *volume-force* frame

$$m_{vf}V_\epsilon'' + b_{vf}V_\epsilon' + k_{vf}V_\epsilon = Fe^{i\omega t} \tag{4}$$

where m, b and k being the effective mass, effective damping coefficient and effective spring constant of the system. Assuming that bubbles are acoustically compact ($KR_0 \ll 1$) sound sources, force can be related to the pressure on the surface of the bubble as

$$F = P4\pi R_0^2 \tag{5}$$

Making another assumption that the bubble shape is spherical and the oscillation amplitude is assumed to be small, change in volume of the bubble $dV = V_\epsilon$ can be linearized about the equilibrium value R_0 as

$$V_\epsilon = dV = 4\pi R_0^2 dR = 4\pi R_0^2 R_\epsilon \tag{6}$$

Using the relations in Equations (5,6) one can relate the coefficients for mass, spring constant damping coefficient in different frames of reference used in Equations (1-4).

2.2 Stiffness

The gas within the bubble acts as a spring by changing its pressure as it contracts and expands. If the gas can be modeled to follow a polytropic law $PV^\gamma = constant$, then for a small change (increase) in volume dV, the change (decrease) in pressure is

$$dP = -\gamma P_0 \frac{dV}{V_0} \tag{7}$$

where P_0 is the equilibrium pressure. The force acting on the bubble due to this change in pressure is $F = 4\pi R_0^2 dP$. Using this relation with the relations in Equations (5,7), force can be related to change in radius as $F = -12\pi R_0 P_0 R_\epsilon$. Hence from the analogy of a spring ($F = -kx$), the equivalent stiffness of the bubble in the *radius-force* frame can be derived as

$$k_{rf} = 12\pi\gamma R_0 P_0 \tag{8}$$

Using the relations in Equations (5,6), we can express the stiffness in other frames of reference as $k_{rp} = k_{vf} = \frac{3\gamma}{R_0}P_0$ and $k_{vp} = \frac{\gamma}{V_0}P_0$.

2.3 Inertia

In class it was shown that for a pulsating sphere, surrounding fluid can be assumed to be incompressible for small distances from the surface of the sphere. The incompressibility condition means that the flux $\vec{u}A$ is constant on a spherical shell around the sphere. Hence a pulsating bubble would setup a significant amount of liquid around it into motion, which contributes to the inertia of the system. Specific acoustic impedance for a pulsating sphere emitting spherically symmetric radial waves in the compact limit is given by $Z = \rho_0 c_0[(KR_0)^2 + i(KR_0)]$ (derived in class). We can define a related quantity, radiation impedance (Z^{rad}) as the ratio of force to particle velocity, hence $Z^{rad} = Z4\pi R_0^2$. Hence the inertia of this system in the *radius-force* frame is then given by

$$m_{rf} = Im\{Z^{rad}\}/\omega = \rho 4\pi R_0^3 \tag{9}$$

Using the relations in Equations (5,6), we can express the effective mass in other frames of reference as $m_{rp} = m_{vf} = \rho R_0$ and $m_{vp} = \frac{\rho}{4\pi R_0}$.

2.4 Damping

The real part of Z^{rad} is the resistive contribution, $b_{rf} = 4\pi R_0^2 \rho_0 c_0 (KR_0)^2$ and is responsible for the damping that results from the radiation of energy away from the bubble as sound. Thermal conduction and viscous dissipation also contributes to damping (Leighton 2012) and the derivation of relations for those are beyond the scope of this report.

We can thus define the resonance frequency (Minnaert frequency) of the bubble (analogous to spring-mass system) as

$$\omega = \sqrt{\frac{k_{rf}}{m_{rf}}} = \frac{1}{R_0}\sqrt{\frac{3\gamma P_0}{\rho}} \tag{10}$$

which was first derived by Minnaert (1933) based on energy arguments. The effect of surface tension is known to change the frequency by modifying the effective stiffness coefficient (see, Appendix A).

3 Non-spherical bubble oscillations

Lamb (1932) studied the shape oscillations of inviscid drop immersed in a fluid. Following his analysis, suppose there is bubble of radius of R_0 in a fluid of density ρ and the shape of the bubble be perturbed in an oscillatory fashion ε, given by

$$R(t) = R_0 + \varepsilon(\theta, \phi, t) = R_0 + A_n Y_n^0 cos(\omega_n t) \tag{11}$$

where Y_n^0 is the zonal spherical harmonic of mode n, A_n is the amplitude and ω_n is the temporal oscillation frequency. In the incompressible limit, the linearized wave equation reduces to Laplace equation for velocity potential. Hence using the method of separation of variables, the radial component equation can be derived as

$$\frac{1}{r^2}\frac{\partial}{\partial r}\Big(r^2\frac{\partial \phi_r}{\partial r}\Big) - \frac{n(n+1)}{r^2}\phi_r = 0 \tag{12}$$

and solving this, we can obtain the velocity potential outside the bubble as

$$\phi = \frac{\omega_n R_0}{n+1}\Big(\frac{R_0}{r}\Big)^{n+1} A_n Y_n^0 sin(\omega_n t) \tag{13}$$

that satisfies the boundary condition for the radial wall velocity

$$\frac{\partial \varepsilon}{\partial t}|_{r=R_0} = \frac{\partial \phi}{\partial t}|_{r=R_0} \tag{14}$$

Now, calculating the acoustic pressure, we obtain

$$p = -\rho\frac{\partial \phi}{\partial t} = -\frac{\rho\omega_n^2 R_0}{n+1}(\frac{R_0}{r})^{n+1} A_n Y_n^0 cos(\omega_n t) \tag{15}$$

Hence the pressure emitted by the zeroth mode ($n = 0$) decays as r^{-1} (a monopole), whereas for higher order modes ($n > 1$), pressure field decays much quicker as $r^{-(n+1)}$ and hence are more weaker when compared to the zeroth mode. However, Longuet-Higgins (1989) extended this study with second-order perturbation theory and showed that the second-order terms results in a monopole radiation (r^{-1}) for higher order modes. But there is no experimental evidence supporting this multi-frequency emission behavior for bubbles (Medwin & Beaky 1989) in real world forcing conditions. Hence this behavior of multi-frequency emission by bubbles has been ignored in the subsequent studies.

4 Excitation mechanism: Entrainment

Bubbles are excited during the entrainment process due to a sudden change in the pressure. Figure 1 shows the entrainment process along with the pressures in the bubble at various times. Pressure of the gas inside the bubble is p_{atm} until the surface of the liquid closes, but increases to $p_{atm}+\rho gh+2\sigma/R$ immediately after the liquid surface closes. This increase in pressure compresses the gas and the inertia carried by the surrounding liquid further compresses the bubble to an extent such that a pressure of approximately $p_{atm} + 2(\rho gh + 2\sigma/R)$ is achieved, assuming a linear small-amplitude pulsation. Further, the bubble oscillates back and forth until all the energy is damped.

Hence the far-field pressure can be modeled as $p(r,t) = P_A\frac{R_0}{r}e^{-\beta(t-r/c)}$, where P_A is the pressure amplitude at the bubble wall given by $P_A = (2\sigma/R+\rho gh)e^{i(\omega t-kr)}$. In real world scenarios, entrainment is due to a breaking wave or rainfall on free surface, which entrains bubbles near the water surface and hence this is typically modeled as a dipole given by

$$P(r,\theta,t) = (\frac{2\sigma + \rho ghR_0}{r})2hkcos\theta e^{-\beta(t-k/r)}e^{i(\omega t-kr)} \tag{16}$$

Experimental results by Pumphrey & Elmore (1990) for the entrainment of bubbles in a drop-surface impact problem also matches fairly well with this model prediction.

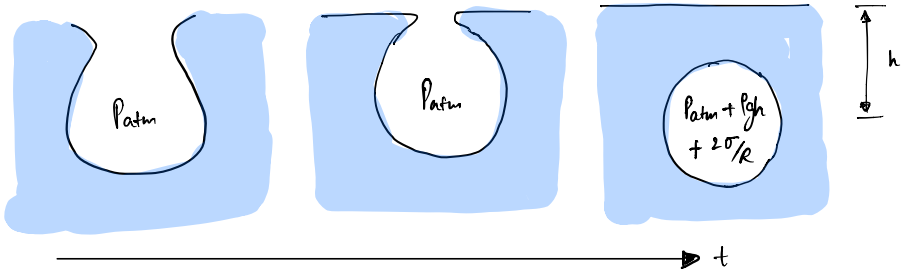

Figure 1: Schematic showing the change in internal pressure of the bubble during the entrainment process.

5 Synthesizing sound from underwater bubbles

5.1 Incompressible fluid simulation

Direct computation of sound from underwater bubbles could be expensive as was already pointed out. Hence an incompressible flow solver is used here to solve for both the phases (air and water). Fluid simulation requires solving an incompressible, variable-density Navier-Stokes equations along with the surface tension

$$\rho(\frac{\partial u}{\partial t} + \vec{u} \cdot \vec{\nabla}\vec{u}) = -\vec{\nabla}p + \vec{\nabla} \cdot (2\mu D) + \sigma K \vec{n} \tag{17}$$

and a volume fraction advection equation $\frac{\partial c}{\partial t} + \vec{\nabla} \cdot (c\vec{u}) = 0$ and a projection method to achieve divergence free condition for the velocity. Where ρ and μ are spatially varying density and viscosity given by $\rho = c\rho_1 + (1-c)\rho_2$ and $\mu = c\mu_1 + (1-c)\mu_2$. We use an open source package Gerris (Popinet 2003) to solve the equations along with the AMR capability to speed up the calculation. An example problem of a falling droplet into a pool of water in a container is chosen as the test case in the present study (see, Appendix B for further details and results).

5.2 Frequency estimation

Then to calculate the frequency of the sound emitted by each bubble using the Equation 10, we need to compute the effective stiffness k using the Equation 8 and an effective mass m (Equation 9). The frequency computed this way do not take into account the effect of near-field geometry and will not in general produce the observed increase in frequency as the bubble rises to the surface (Langlois et al. 2016). Hence a more sophisticated method proposed by Strasberg (1953) is used here, wherein an interior Laplace equation in the liquid region (Figure 2) surrounding the bubble is solved for each bubble to calculate the effective mass m (see, Appendix C for more details on the equations used). This calculation requires the geometry information of the air-water interface (free surface and surface of the bubbles generated due to drop impact) and can be obtained from the solution of the fluid flow solver. Laplace equation can be solved using the boundary integral formulation for the Laplace's equation.

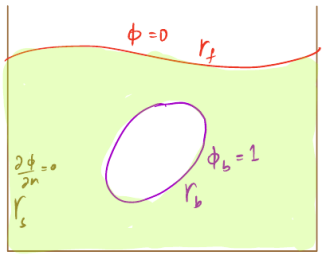

Figure 2: Domain for the solution of interior Laplace equation.

5.3 Radiation

Once the frequency from each of the bubble is computed, an exterior Helmholtz problem ($\vec{\nabla} \cdot p + k^2 p = 0$) can be solved for the radiation of the sound from the air-water interface (free surface) to the listener position (3). Boundary conditions at the free surface can be obtained from the solution of the interior Laplace equation (Section 5.2). To solve exterior Helmholtz BVP, an open-source bempp solver (Śmigaj et al. 2015) can be used. A more challenging, practical task here is to convert the volumetric data obtained from the fluid solver into a surface mesh that can be used in

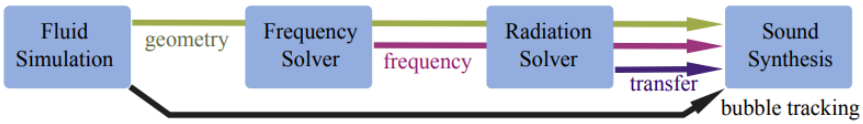

Figure 4: Overview of the bubble sound synthesis techniques.

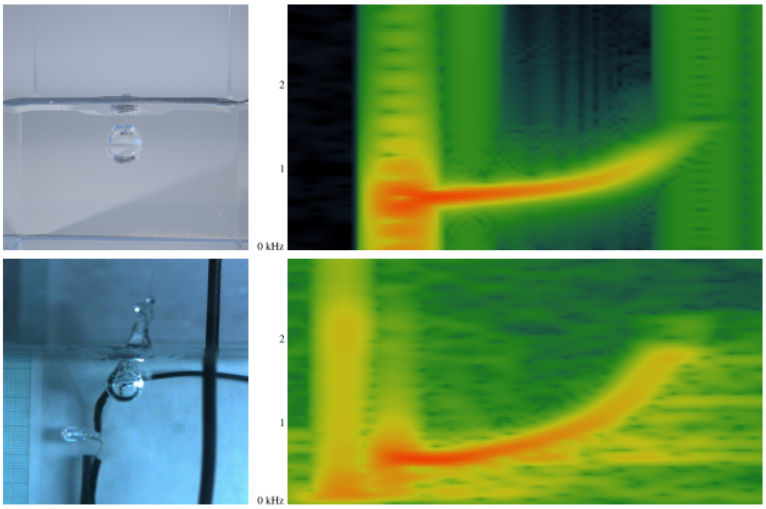

Figure 5: Comparison of frequency response for a single bubble entrainment from the simulation (top) with the experiments (bottom).

the bempp solver. This requires writing plugins to convert the volumetric data from "vtk" format to surface data in "msh" format, which can be achieved in the future.

Bempp is a C++ library that uses Galerkin discretizations of boundary integral equations to solve Laplace, Helmholtz and Maxwell equations. A sample solution of scattering of sound solved using bempp is included in Appendix D for the illustration of capability to solve Helmholtz equation.

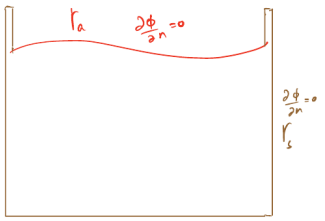

Figure 3: Domain for the solution of exterior Helmholtz problem.

5.4 Synthesis

Additionally, the excitation of the bubble during the process of entrainment, bubble breakup, coalescence and popping can be modeled as forces that are active for a short period of time. Langlois et al. (2016) lists the forces used to model these phenomenon, that are estimated from previous experimental studies. Hence after every time step of the fluid simulation, the bubble geometry is processed to detect entrainment, breakup, coalescence and popping phenomenon. The appropriate forcing functions are activated and the frequencies are estimated and the radiation is solved. Figure 4 summarizes, the process of synthesizing sound generated from underwater bubbles using incompressible fluid simulation techniques.

Frequency response from the simulation of a single bubble entrainment, as computed by Langlois et al. (2016) is compared against the experimental measurement in Figure 5 and shows the high accuracy of the prediction obtained from the model.

6 Summary

Direct computation of sound from the bubbles underwater is expensive. This warrants the development of alternate methods to compute sound. Hence, the prediction of sound generated by bubbles using reduced-order models along with an incompressible fluid flow solver is computationally less expensive. This report includes the summary of derivation of such models along with the procedure to synthesize sound developed by Langlois et al. (2016).

References

Lamb, H. (1932), *Hydrodynamics*, Cambridge university press.

Langlois, T. R., Zheng, C. & James, D. L. (2016), 'Toward animating water with complex acoustic bubbles', *ACM Transactions on Graphics (TOG)* **35**(4), 95.

Leighton, T. (2012), *The acoustic bubble*, Academic press.

Longuet-Higgins, M. S. (1989), 'Monopoly emission of sound by asymmetric bubble oscillations. part 1. normal modes', *Journal of Fluid Mechanics* **201**.

Medwin, H. & Beaky, M. M. (1989), 'Bubble sources of the knudsen sea noise spectra', *The Journal of the Acoustical Society of America* **86**(3), 1124–1130.

Minnaert, M. (1933), 'Xvi. on musical air-bubbles and the sounds of running water', *The London, Edinburgh, and Dublin Philosophical Magazine and Journal of Science* **16**(104), 235–248.

Popinet, S. (2003), 'Gerris: a tree-based adaptive solver for the incompressible euler equations in complex geometries', *Journal of Computational Physics* **190**(2), 572–600.

Pumphrey, H. C. & Elmore, P. A. (1990), 'The entrainment of bubbles by drop impacts', *Journal of Fluid Mechanics* **220**.

Rayleigh, L. (1917), 'On the pressure developed in a liquid during the collapse of a spherical cavity: Philosophical magazine series 6, 34, 94–98'.

Śmigaj, W., Betcke, T., Arridge, S., Phillips, J. & Schweiger, M. (2015), 'Solving boundary integral problems with bem++', *ACM Transactions on Mathematical Software (TOMS)* **41**(2), 6.

Strasberg, M. (1953), 'The pulsation frequency of nonspherical gas bubbles in liquids', *The Journal of the Acoustical Society of America* **25**(3), 536–537.

Appendix A:- Effect of surface tension.

Effective stiffness in volume - pressure frame is,

$$K_{vp} = -\frac{\partial P_L}{\partial V}$$ ← pressure at the bubble wall.

Pressure inside the bubble is given by,

$$P_i(t) = P_L + \frac{2\sigma}{R(t)}$$ → surface tension.

From polytropic law

$$\frac{P_i(t)}{\left(P_0 + \frac{2\sigma}{R_0}\right)} \times \left(\frac{V(t)}{V_0}\right)^{\gamma} = \text{constant}$$

$$\Rightarrow \quad \frac{P_L + \frac{2\sigma}{R(t)}}{P_0 + \frac{2\sigma}{R_0}} = \left(\frac{V_0}{V(t)}\right)^{\gamma}$$

$$\Rightarrow \quad P_L = \left(P_0 + \frac{2\sigma}{R_0}\right)\left(\frac{V_0}{V(t)}\right)^{\gamma} - \frac{2\sigma}{R(t)}$$

$$\therefore K_{vp} = -\frac{\partial P_L}{\partial V} = \frac{\gamma P_0}{V_0}\left(1 + \frac{2\sigma}{P_0 R_0} - \frac{2\sigma}{3\gamma P_0 R_0}\right)$$

∴ The resonance frequency is

$$\omega = \frac{1}{R_0}\sqrt{\frac{3\gamma P_0}{\rho}\left(1 + \frac{2\sigma}{P_0 R_0}\right) - \frac{2\sigma}{\rho R_0}}$$

Appendix B: Fluid simulation of a falling drop using Gerris

A falling drop was simulated with a density of 1000 for water, 1 for air, viscosity of 10^-5 for both the phases, surface tension of 0.072, gravity of 9.81. Non-dimensional initial radius of the drop is $r = 1/12$ and is initially located a distance of $2r$ from the free surface.

Using the AMR capability, grid was refined closest to the interfaces and had an equivalent resolution of 128^3. Simulation was performed in serial on the local workstation and took around $8hrs$ to complete. Input script used to perform the simulation is included below along with results in the Figure below.

```
1 0 GfsSimulation GfsBox GfsGEdge {} {
    Global {
  #define radius 1./12.
  #define h 2./12.
  #define rho(T) (1000.*T + (1. - T))
    }
    Time { end = 10 }
      # Initial refinement
    Refine 5

      VariableTracerVOF T
      InitFraction {} T ({
    double drop = radius*radius - (x*x + (y-radius)*(y-radius) + z*z);
    double fs = y + h;
    return intersection(drop,-fs);
  })
      VariableCurvature K T Kmax
      SourceTension T 0.072 K
      PhysicalParams { alpha = 1./rho(T) }

  AdaptGradient {istep = 1} { maxlevel = 7 cmax = 1e-2 } T

  SourceViscosity {} 0.00001

  Source {} V -9.81

    # Dynamic load-balancing
    EventBalance { istep = 1 } 0.1

  OutputTime { istep = 1 } log
      OutputBalance { istep = 1 } log
      OutputProjectionStats { istep = 1 } log
      OutputTiming { istep = 100 } log

  GModule gfsview
      OutputView { step = 4e-3 } { ppm2theora -s 2048x1080 > falling_drop.ogv } {
  format = PPM width = 2048 height = 1080
      } falling_drop.gfv

    # Save a (single) snapshot every 100 timesteps
    OutputSimulation { istep = 1 } snapshot-%ld.gfs { }
    OutputSimulation { istep = 1 } snapshot-%ld.vtk {format=VTK}
    OutputSimulation { istep = 1 } stdout

}
GfsBox {}
```

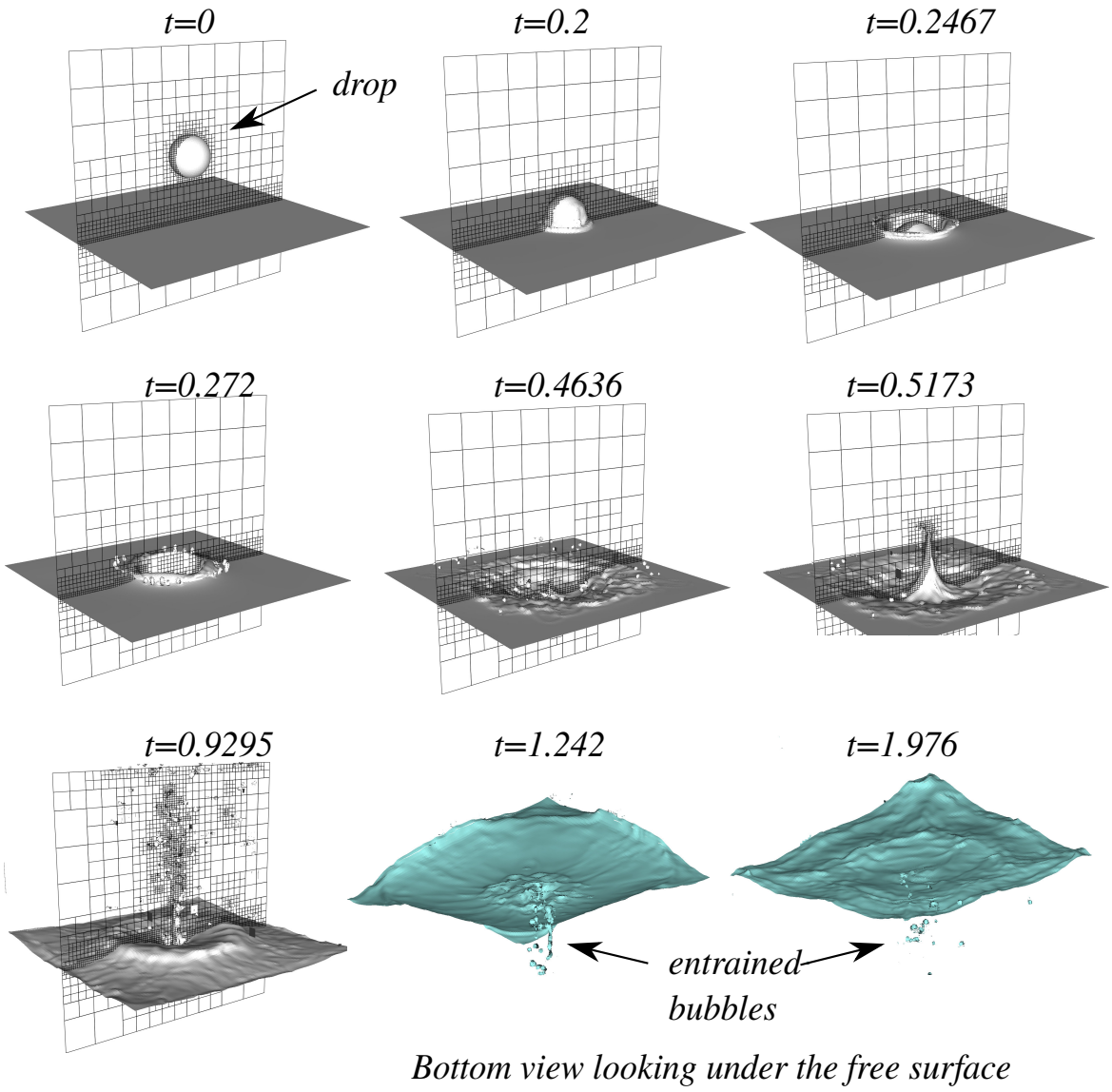

Figure 1: Results of the simulation of a falling droplet, showing the bubbles entrained.

Appendix C :- Procedure to calculate Radiation mass (effective mass)

Equating kinetic energy of the oscillator to the kinetic energy of the surrounding fluid.

$$\Rightarrow \quad \frac{1}{2} m_{rad} \dot{v}^2 = KE_f$$

In volume-pressure plane, units of $m_{rad} \sim \frac{l}{\dot{v}} \sim \frac{N}{m^2 \times m^3} t^2 \sim \frac{\text{mass}}{(\text{area})^2}$

→ Bubbles are compact sources ⇒ Surrounding fluid is incompressible and irrotational.
(ka = 0.0136)

Hence it satisfies,

$$\therefore \quad \vec{\nabla}^2 \phi(\vec{x}) = 0 \qquad \text{for } \vec{x} \in \Omega$$

Solving for ϕ,

$$\therefore \quad KE_f = \frac{\rho}{2} \int_\Omega (\vec{\nabla}\phi)^2 \, d\Omega$$

$$\Rightarrow \quad \boxed{m_{eff} = \frac{\rho}{\dot{v}^2} \int_\Omega (\vec{\nabla}\phi)^2 \, d\Omega}$$

Green's first identity :-

$$\int \vec{\nabla}.F \, dv = \int \vec{F}.\vec{n} \, ds$$

if $\vec{F} = \phi \vec{\nabla}\phi$ $\quad \int \vec{\nabla}.(\phi \vec{\nabla}\phi) \, dv = \int (\phi \vec{\nabla}\phi).\vec{n} \, ds$

$$\Rightarrow \int_V (\vec{\nabla}\phi).(\vec{\nabla}\phi) \, dv + \int_V \phi \vec{\nabla}^2 \phi \, dv = \int_S \phi (\vec{\nabla}\phi).\vec{n} \, ds$$

Using this for above problem,

$$\int_\Omega (\vec{\nabla}\phi)^2 \, d\Omega + \int_\Omega \phi (\vec{\nabla}^2 \phi) \, d\Omega = \int_{\partial\Omega} \phi \frac{\partial \phi}{\partial n} \, ds$$

($\vec{\nabla}^2\phi = 0$)

→ Hence to compute ϕ, an interior Laplace problem needs to be solved.

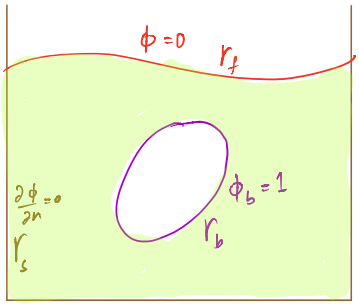

→ To solve laplace equation in this region, boundary conditions are,

ⓐ free surface (Γ_f)

Water	Air
Z_1	Z_2

$$\Pi = \frac{2 Z_2}{Z_2 + Z_1}$$

$$Z_2 << Z_1$$

$$\Rightarrow \Pi \approx 0 \Rightarrow p \approx 0 \text{ at the surface}$$

(pressure release surface)

$$\therefore p = -\rho_0 \frac{\partial \phi}{\partial t} = i\omega \rho_0 \phi = 0$$

$$\therefore \phi = 0 \text{ is the BC at } \Gamma_f$$

ⓑ Rigid walls (Γ_s)

$$u_n = 0 \Rightarrow \frac{\partial \phi}{\partial n} = 0 \text{ is the BC at } \Gamma_s$$

ⓒ Bubble surface (Γ_b)

$$p = -\rho_0 \frac{\partial \phi}{\partial t} = i\omega \rho_0 \phi$$ [Uniform on the surface of the bubble]

$$\phi = \phi_b \text{ at } \Gamma_b$$

Once the interior Laplace equation is solved,

$$m_{rad} = \frac{\rho}{\dot{v}^2}\int_{\Omega}(\vec{\nabla}\phi)^2\, d\Omega = \frac{\rho}{\dot{v}^2}\left\{\int_{r_b}\phi\,\frac{\partial\phi}{\partial n}\,ds + \int_{r_s}\phi\,\frac{\partial\phi}{\partial n}\,ds + \int_{r_t}\phi\,\frac{\partial\phi}{\partial n}\,ds\right\}$$

$\therefore\ m_{rad} = m_b$ [Only contribution from the bubble surface].

$$= \frac{\rho\,\phi_b}{\dot{v}^2}\int_{r_b}\frac{\partial\phi}{\partial n}\,ds$$

Volume velocity is given by $\dot{v} = \int_{r_b}\frac{\partial\phi}{\partial n}\,ds$

$\Rightarrow$

$$\boxed{m_{rad} = \frac{\rho\,\phi_b}{\dot{v}}}$$

Solving the Laplace equation, $\dot{v}$ can be computed and hence m_{rad}.

Appendix D: Solution of scattering from a unit sphere

Let the incident wave be $u^{\text{inc}}(\mathbf{x}) = e^{ikx}$

and the governing equation is the Helmholtz equation $\Delta u + k^2 u = 0$

where $u = u^s + u^{\text{inc}}$ is the total acoustic field and u^s satisfies the Sommerfeld radiation condition.

```
In [ ]: import bempp.api
        import numpy as np

In [2]: #wavenumber
        k = 15.

In [3]: #spherical mesh
        grid = bempp.api.shapes.regular_sphere(5)

In [4]: #piecewise constant basis function
        piecewise_const_space = bempp.api.function_space(grid, "DP", 0)

In [6]: #intialising boundary operators
        identity = bempp.api.operators.boundary.sparse.identity(
            piecewise_const_space, piecewise_const_space, piecewise_const_space)
        adlp = bempp.api.operators.boundary.helmholtz.adjoint_double_layer(
            piecewise_const_space, piecewise_const_space, piecewise_const_space, k)
        slp = bempp.api.operators.boundary.helmholtz.single_layer(
            piecewise_const_space, piecewise_const_space, piecewise_const_space, k)

        lhs = 0.5 * identity + adlp - 1j * k * slp

In [7]: #defining rhs
        def combined_data(x, n, domain_index, result):
            result[0] = 1j * k * np.exp(1j * k * x[0]) * (n[0]-1)

        grid_fun = bempp.api.GridFunction(piecewise_const_space, fun=combined_data)

In [8]: #using gmres to solve
        from bempp.api.linalg import gmres
        neumann_fun, info = gmres(lhs, grid_fun, tol=1E-5)
```

In [10]:
```
#choosing the domain of interest

Nx = 200
Ny = 200
xmin, xmax, ymin, ymax = [-3, 3, -3, 3]
plot_grid = np.mgrid[xmin:xmax:Nx * 1j, ymin:ymax:Ny * 1j]
points = np.vstack((plot_grid[0].ravel(),
                    plot_grid[1].ravel(),
                    np.zeros(plot_grid[0].size)))
u_evaluated = np.zeros(points.shape[1], dtype=np.complex128)
u_evaluated[:] = np.nan
```

In [11]:
```
#evaluating solution in the domain of interest
x, y, z = points
idx = np.sqrt(x**2 + y**2) > 1.0

from bempp.api.operators.potential import helmholtz as helmholtz_potential
slp_pot = helmholtz_potential.single_layer(
    piecewise_const_space, points[:, idx], k)
res = np.real(np.exp(1j *k * points[0, idx]) - slp_pot.evaluate(neumann_fun))
u_evaluated[idx] = res.flat
```

In [17]:
```
#plot the solution
%matplotlib inline

u_evaluated = u_evaluated.reshape((Nx, Ny))

from matplotlib import pyplot as plt
fig = plt.figure(figsize=(10, 8))
plt.imshow(np.real(u_evaluated.T), extent=[-3, 3, -3, 3])
plt.xlabel('x')
plt.ylabel('y')
plt.colorbar()
plt.title("Scattering from the unit sphere, solution shown in the plane z=0")
```

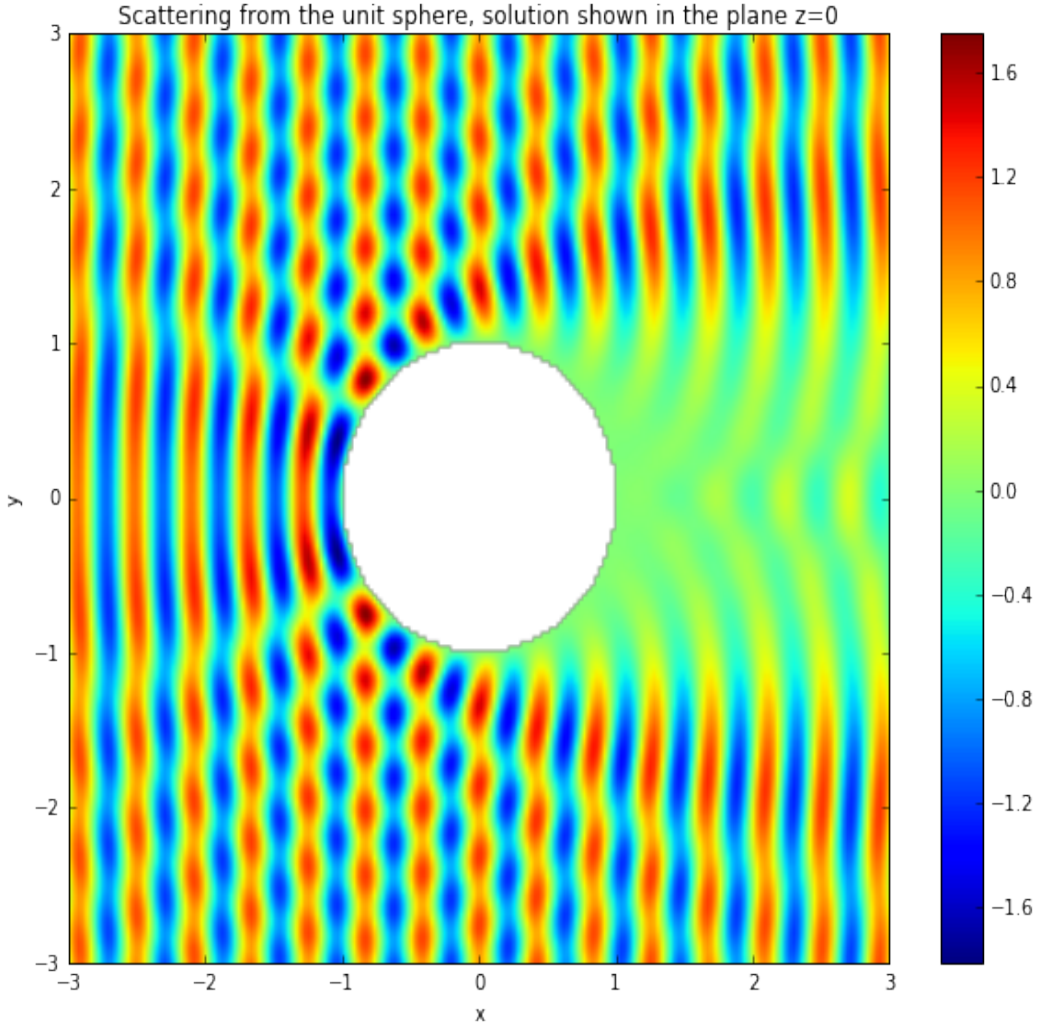
Scattering from the unit sphere, solution shown in the plane z=0
3
2
1
0
−1
−2
−3
y
−3
−2
−1
0
1
2
3
x
1.6
1.2
0.8
0.4
0.0
−0.4
−0.8
−1.2
−1.6